Polymer Chemistry

ROYAL SOCIETY OF CHEMISTRY

PAPER

View Article Online
View Journal | View Issue

Check for updates

Cite this: *Polym. Chem.*, 2026, **17**, 207

Simultaneous interpenetrating network (SIN) hydrogels from poly(sarcosine) and poly(ethylene glycol) (PEG)

Guonan Ji,[a,b] Shan An,[c,d] Gianluca Bartolini Torres,[a,e] Fergal J. O'Brien,[c,f] Ziyuan Song,[b] Bo Li*[a,f] and Andreas Heise *[a,e,f]

Received 28th October 2025,
Accepted 3rd December 2025

DOI: 10.1039/d5py01018g

rsc.li/polymers

Hydrogels are widely employed in biomedical applications such as drug delivery, tissue engineering, and wound healing due to their ability to mimic the properties of biological tissues. Here, the development of novel simultaneous interpenetrating network (SIN) hydrogels composed of polysarcosine (PSar) and polyethylene glycol (PEG), crosslinked through orthogonal photochemical reactions is reported. The PSar single network was formed by free-radical polymerization of methacrylate-functionalized PSar, while the second network was generated simultaneously from cinnamic acid-modified PEG *via* [2 + 2] cycloaddition. Comprehensive characterization revealed that the SIN hydrogels exhibit enhanced mechanical performance, including higher elongation at break, ultimate tensile strength, compressive strength, fracture strain, and Young's modulus, compared to the individual networks. Furthermore, rat mesenchymal stem cell assays confirmed superior cytocompatibility, with robust metabolic activity and proliferation on SIN hydrogels. Collectively, these findings demonstrate that PSar-based SIN hydrogels combine mechanical robustness with biocompatibility, highlighting their strong potential as functional materials for artificial tissue applications.

Open Access Article. Published on 03 decembar 2025. Downloaded on 16.5.2026. 03.44.44.
This article is licensed under a Creative Commons Attribution 3.0 Unported Licence.

Introduction

Hydrogels are three-dimensional, cross-linked polymeric networks capable of retaining large amounts of water.[1–4] Owing to their high water content, tuneable permeability, and structural similarity to the extracellular matrix (ECM), hydrogels are preferred biomaterials for applications such as tissue engineering scaffolds.[5–8] Natural polymers, for example hyaluronic acid, alginate, and gelatine, are commonly used in hydrogel fabrication due to their excellent biocompatibility and low immunogenicity.[9–15] However, synthetic hydrophilic polymers like polyacrylamide (PAM), poly(vinyl alcohol) (PVA) and poly(ethylene glycol) (PEG) offer greater chemical versatility, mechanical tunability, and consistent synthesis, making them an attractive choice for a broad range of bioengineering applications.[16–22] PEG is particularly popular in these applications for its ability to minimize protein adsorption, and its compatibility with growth media.[23–26] However, its widespread use has come under increasing scrutiny as growing evidence links PEGylated products to enhanced immune responses.[27–29]

In recent years, polysarcosine (PSar) has emerged as a promising alternative to PEG in various biomedical applications, including drug delivery and tissue engineering, due to its excellent biocompatibility and non-immunogenicity.[30–33] PSar is a hydrophilic polypeptoide that can be synthesised *via* the ring-opening polymerisation of sarcosine *N*-carboxyanhydride (NCA), a *N*-substituted derivative of the natural amino acid glycine.[34,35] The potential of PSar-based hydrogels in tissue repair has been demonstrated in a recent study.[36] It was shown that enhanced early-stage *in vivo* cartilage and bone regeneration can be achieved by modulating immune responses, mitigating foreign body reactions, and promoting ECM deposition. These advantages position PSar-based hydrogels as a highly promising platform for tissue engineering applications.

One challenge in the development of hydrogel materials for tissue applications is optimising their mechanical properties to improve cell interaction, structural stability, and long-term

[a]*Department of Chemistry, RCSI University of Medicine and Health Sciences, Dublin 2, Ireland. E-mail: andreasheise@rcsi.ie*
[b]*Institute of Functional Nano & Soft Materials (FUNSOM), Jiangsu Key Laboratory for Carbon-Based Functional Materials and Devices, Joint International Research Laboratory of Carbon-Based Functional Materials and Devices, Soochow University, Suzhou 215123, China*
[c]*Tissue Engineering Research Group (TERG), Department of Anatomy and Regenerative Medicine, RCSI University of Medicine and Health Sciences, Dublin 2, Ireland*
[d]*College of Pharmaceutical Sciences, Soochow University, Suzhou 215123, China*
[e]*Research Ireland Centre for Research in Medical Devices (CURAM), RCSI, Dublin 2, Ireland*
[f]*AMBER, The Research Ireland Advanced Materials and Bioengineering Research Centre, RCSI, Dublin 2, Ireland*

Open Access Article. Published on 03 decembar 2025. Downloaded on 16.5.2026. 03.44.44.
This article is licensed under a Creative Commons Attribution 3.0 Unported Licence.

durability.[37,38] To address this, crosslinking strategies are commonly applied.[39–42] Another strategy for enhancing hydrogel performance is the development of interpenetrating polymer network (IPN) hydrogels, which consist of two or more physically interlaced but chemically distinct polymer networks.[43–49] This unique architecture imparts exceptional toughness, elasticity, and damage tolerance to the hydrogels. IPNs can be synthesised through either sequential or simultaneous formation of the constituent networks. A widely used approach is the simultaneous interpenetrating network (SIN) strategy, which involves the concurrent polymerisation of two distinct monomer/crosslinker systems.[50–52] Successful SIN formation requires precise control over the crosslinking kinetics and polymerisation mechanisms to ensure non-interfering, independently formed networks. For example, photo-initiated acrylate polymerisation was combined with thermally activated epoxy curing, whereby rapid photo-polymerisation forms the primary network, while slower thermal curing establishes the secondary network.[53] In another reported system, an IPN derived from cationic ring-opening polymerisation (CROP) of mono- and difunctional oxazolines, coupled with reversible addition–fragmentation chain transfer (RAFT) polymerisation of acrylamides was reported.[54] In both examples, the employed polymerisation techniques are mechanistically and temporally distinct, leading to the formation of individual networks on different time scales.

Herein, we present a novel strategy for the fabrication of PSar/PEG IPN hydrogels *via* a SIN approach. This method leverages the combination of two structurally distinct yet functionally similar polymers both recognised for their biocompatibility, stealth properties, and hydrophilicity. We hypothesised that integrating these polymers into a single IPN architecture would yield enhanced properties not attainable by either network alone. In our design, photo-polymerisation initiates the formation of both networks concurrently, yet through orthogonal mechanisms and at distinct timescales. The first network is constructed from methacrylate-functionalised PSar, crosslinked *via* free-radical polymerisation, while the second network arises from cinnamic acid-modified PEG, crosslinked through a [2 + 2] photochemical cycloaddition reaction. This orthogonal crosslinking strategy enables independent yet simultaneous network formation, resulting in efficient polymerisation and tuneable mechanical properties. The PEG/Sar networks outperform their individual networks in both mechanical properties (tensile and compression strength) and display an 2–3 fold enhanced cell seeding efficiency.

Experimental

Materials

All chemicals were purchased from Sigma-Aldrich (St Louis, USA) and used as received unless otherwise specified. Boc-sarcosine, $MgSO_4$, and NaCl were obtained from Fluorochem Ltd, UK. 4-Arm poly(ethylene glycol) derivative (pentaerythritol core) (PEG-OH, 2000 g mol^{-1}) was purchased from JenKem Technology USA Inc. 2-Isocyanatoethyl methacrylate, phenylbis (2,4,6-trimethylbenzoyl)phosphine oxide (BAPO), 4-dimethylaminopyridine (DMAP), and propylene oxide were obtained from Tokyo Chemical Industry Co., Ltd.

Synthesis of sarcosine *N*-carboxyanhydride (Sar-NCA). To a 500 mL flask, Boc-sarcosine (10.0 g, 52.9 mmol, 1.0 eq.), acetonitrile (200 mL), propylene oxide (36 mL, 529 mmol, 10.0 eq.) were added sequentially into a flask under magnetic stirring in an ice bath. Triphosgene (7.85 g, 26.4 mmol, 0.5 eq.) was added in one portion and the flask was left open to the atmosphere to allow the release of CO_2 generating during *in situ* BOC deprotection. The reaction was stirred at 0 °C in an ice bath for 1.5 h. Then the excessive triphosgene was quenched by adding cold water (100 mL) with 1–3 min stirring. The mixture was extracted with ethyl acetate (200 mL × 2) at room temperature. The combined organic phase was washed with brine and dried with anhydrous $MgSO_4$. After the removal of solvent by rotatory evaporation under vacuum, the crude product was purified by crystallization in hexane/THF at −20 °C. Pure Sar-NCA was obtained as a white needle crystal (Yield: 53%). ^{1}H NMR (400 MHz, DMSO-d_6, 299 K, ppm): δ = 4.21 (s, 2H, C***H*****$_2$**CO), 2.86 (s, 3H, C***H*****$_3$**) ppm.

Synthesis of di-amino polysarcosine (PSar). Sar-NCA (2.0 g, 17.4 mmol) was dissolved in DCM (31 mL), into which the DCM solution of 1,6-hexanediamine (C6-diNH_2) (0.1 M, 12.4 mL, $[M]_0/[I]_0$ = 28) was added. The polymerization was left under stirring for 2 h at room temperature until complete conversion of NCA as monitored by FTIR. The product PSar was purified by precipitation in diethyl ether and dried under vacuum (Yield: 87%). ^{1}H NMR (400 MHz, DMSO-d_6, 299 K, ppm): δ = 4.57–3.73 (m, 56H, C***H*****$_2$**CO), 3.20–2.68 (m, 84H, C***H*****$_3$**) ppm, 1.52–1.05 (m, 8H, C***H*****$_2$**).

Chain-end modification of di-amino polysarcosine with 2-isocyanatoethyl methacrylate. Polysarcosine (1.0 g, 0.47 mmol, 1.0 eq.) was dissolved in DMF (10 mL). Then 2-isocyanatoethyl methacrylate (189.6 mg, 1.22 mmol, 2.6 eq.) was added, and the mixture was stirred at 40 °C overnight. The product methacrylate-modified polysarcosine (PSar-MA) was purified by precipitation in diethyl ether and dried under vacuum (Yield: 83%). ^{1}H NMR (400 MHz, DMSO-d_6, 299 K, ppm): δ = 6.06 and 5.67 (s, 4H, C***H*****$_2$**═C(CH_3)COO), 4.57–3.73 (m, 56H, C***H*****$_2$**CO), 3.20–2.68 (m, 84H, C***H*****$_3$**), 1.88 (s, 6H, CH_2═C(*C****H*****$_3$**)COO) ppm, 1.52–1.05 (m, 8H, C***H*****$_2$**).

Synthesis of cinnamic acid-modified 4 arm PEG. 4-Arm PEG-OH (2 kDa, 1.0 g, 0.5 mmol, 1.0 eq.), DMAP (63.53 mg, 0.52 mmol, 1.04 eq.) and cinnamic acid (385.21 mg, 2.6 mmol, 5.2 eq.) were dissolved in DCM (20 mL) in an ice bath under nitrogen atmosphere. DCC (536.47 mg, 2.6 mmol, 5.2 eq.) was dissolved in DCM (5 mL) and added dropwise. The solution was stirred at room temperature for 48 h. The white precipitate formed during the reaction was filtered. The filtrate was concentrated under reduced pressure using a rotary evaporator, then precipitated in diethyl ether. The final product (4-arm PEG-CA) was vacuum-dried at 40 °C (Yield: 85%). ^{1}H NMR (400 MHz, $CDCl_3$, 299 K, ppm): δ = 7.76–7.64 (m, 4H, C***H***═CH), 7.57–7.47 (m, 8H, ***Ar***), 7.43–7.32 (m, 12H, ***Ar***),

 This journal is © The Royal Society of Chemistry 2026

Open Access Article. Published on 03 decembar 2025. Downloaded on 16.5.2026. 03.44.44.
This article is licensed under a Creative Commons Attribution 3.0 Unported Licence.

6.52–6.42 (m, 4H, CH═C***H***), 4.49–4.19 (m, 8H, C***H₂***O), 3.84–3.74 (m, 8H, C***H₂***O), 3.73–3.31 (m, 172H, C***H₂***C***H₂***O) ppm.

Cell seeding efficiency

Rat bone marrow-derived mesenchymal stem cells (MSCs) were isolated from 6 to 8 weeks old female Sprague Dawley rats (authorized by Research Ethics Committee of the Royal College of Surgeons in Ireland; application number REC202012003) using standardized protocols and including a stringent analysis of cell phenotype as previously described.[55,56] Cells were expanded in culture and used for experiments at passage 5. rMSCs were counted and seeded at a cell density of 5×10^5 cells per hydrogel (cylinder with a diameter of 10 mm and height of 3.5 mm). Following this, growth medium was added (1 mL per well) and the cells were pre-cultured for 24 h. The cell-seeded hydrogels were transferred to a new 24-well plate after 24 h. Leftover cells attached to the bottom of each well during the seeding procedure were detached and counted using a haemocytometer.

To determine the cell metabolic activity and viability on the hydrogels, an alamarBlue assay was performed on the hydrogels. All hydrogels were washed in a solution of PBS at 24 h prior to any testing and cell analysis, to ensure excess material was removed and the networks environment resembles an *in vivo* setting (*i.e.* aqueous conditions). Metabolic activity of rMSCs in the hydrogel was assessed on day 1, 3, 7, and 10 using an alamarBlue assay (Biosciences, Ireland) according to the manufacturer's instructions. Growth media, consisting of high-glucose Dulbecco's modified Eagle's medium (DMEM) (Sigma-Aldrich, Ireland) supplemented with fetal bovine serum (FBS) (20%, v/v, ThermoFisher Scientific, Ireland), primocin (0.002%, v/v, ThermoFisher Scientific, Ireland), GlutaMAX (1%, v/v, ThermoFisher Scientific, Ireland), and non-essential amino acids (1%, v/v, ThermoFisher Scientific, Ireland) and alamarBlue solution (10%) was added at 37 °C and incubated for 2 h. A spectrophotometer (Wallac 1420 Victor2 D, USA) with an excitation wavelength of 550 nm and an emission wavelength of 590 nm was used to measure the resulting fluorescence levels. Growth media containing 10% alamarBlue was used as a blank sample, and its fluorescence reading was subtracted from the experimental readings to eliminate background fluorescence.

Methods

^{1}H nuclear magnetic resonance (^{1}H NMR) and ^{1}H diffusion ordered (DOSY). Spectra were recorded using a Bruker Avance 400 (400 MHz) spectrometer at room temperature. The chemical shifts (δ) were reported in ppm and referenced to the residual protons in the deuterated solvents. MestReNova software (version 12.0.0, Mestrelab Research, Escondido, USA) was used for all NMR analysis.

Fourier transform infrared attenuated total reflectance spectra (FTIR). Fourier transform infrared attenuated total reflectance spectra (FTIR): were measured on a spectrometer (Thermo Scientific Nicolet iS10) in the spectral region of 500–4000 cm^{-1}.

Size exclusion chromatography (SEC). Molecular weights and polydispersity indices ($Đ = M_w/M_n$) were determined using two different systems depending on sample solubility. SEC in chloroform ($CHCl_3$) was performed on an Agilent Technologies LC 1200 Series equipped with an Agilent 1260 ISO pump, refractive index detector, and two analytical columns (PSS 100 Å and 1000 Å, both 7 μm, 8 mm × 300 mm). Samples (5 mg mL^{-1} in $CHCl_3$) were filtered through a 0.2 μm Millipore filter prior to injection, and chromatograms were recorded at a flow rate of 1.0 mL min^{-1} at 40 °C. The system was calibrated using linear poly(methyl methacrylate) (PMMA) standards (PSS Polymer Standards Service GmbH). For samples soluble in hexafluoroisopropanol (HFIP), SEC analysis was performed using a PSS SECurity system equipped with a PFG 7 μm 8 × 50 mm precolumn, two analytical columns (PSS 100 Å and 1000 Å, both 7 μm, 8 × 300 mm), and a differential refractive index detector. Measurements were conducted at a flow rate of 1.0 mL min^{-1}, and the system was calibrated against Agilent Easi-Vial linear PMMA standards. Data were processed using PSS winGPC UniChrom software.

Rheology. Experiments were carried out using an Anton Paar MCR 301. The experiments were conducted at room temperature using a Peltier hood to protect the sample from ambient light. A parallel plate of 8 mm diameter was used with a gap length of 1.4 mm and a strain of 1%.

Photorheology. Experiments were carried out using an Anton Paar MCR 301. The machine was equipped with a Thorlabs UV LED light 405 nm (M405L3-C1) and a sample glass plate allowing the passage of light. The experiments were conducted at room temperature using a Peltier hood to protect the sample from ambient light. A parallel plate of 25 mm diameter was used with a gap length of 0.05 mm. Each time point was taken every 10 s through a time sweep experiment with constant oscillations at a fixed frequency of 10 rad s^{-1} with a strain of 0.1%. UV light (6 mW cm^{-2}) was turned on after 60 s.

Swelling tests. Sample for swelling tests were prepared by pouring the resin into rectangular molds (0.8 mm × 10 mm × 20 mm) and irradiated with UV light at 405 nm (2 mW cm^{-2}) overnight at room temperature. Afterward, the cross-linked sheets were dried in a vacuum oven (40 °C) overnight. For the swelling test samples were weighted (initial dry mass W_d). The films were then immersed in excess DI water for 48 h at room temperature, then weighted to obtain the swollen mass (W_s). Next, the swollen samples were dried in freeze dryer for 48 h to measure the dry mass after swelling (W_a). Using the following equations, the gel fraction and swelling ratio were calculated. All the measurements were performed in triplicate. Gel fraction (%) = $W_a/W_d \times 100$. Swelling ratio = $(W_s - W_a)/W_a$.

Tensile tests. Measurements were carried out using a Testometric M100-1CT equipped with a 50 N cell load (LC5) and PG15-50L grips. Rectangular cross-linked sheets were used to perform the measurements, obtained according to those described for the swelling test. Before test, all networks were swelled in water for 48h. A gauge length of 8 mm, pretension of 0.1 N, and test speed of 10 mm min^{-1} were used as parameters for the machine. The tests were performed at room

Open Access Article. Published on 03 decembar 2025. Downloaded on 16.5.2026. 03.44.44.
This article is licensed under a Creative Commons Attribution 3.0 Unported Licence.

temperature. The Young's modulus, elongation at break, and ultimate strength were determined as averages of six independent drawing experiments performed under the same conditions.

Compression test. Compression test: were carried out using a Testometric M100-1CT equipped with a 50 N cell load (LC5) and CPS150 square compression platens. Hydrogels were prepared into cylinders with a diameter of 6 mm and height of 2 mm, and swell in water for 48 h before testing. A preload force of 0.1 N was set, and each test was carried out at a compression speed of 5 mm min^{-1} at room temperature. Each gel was subject to a point-break test to determine the Young's modulus, stress at break and strain at break. All compression tests were repeated 6 times, and an average of data was taken.

Results and discussion

Polymer synthesis

Polysarcosine (PSar) was synthesised *via* ring-opening polymerisation (ROP) of sarcosine *N*-carboxyanhydride (Sar-NCA), using 1,6-hexanediamine as the difunctional initiator in dichloromethane (DCM) (Fig. 1A). Monomer conversion was monitored by FTIR spectroscopy (Fig. S1), where the disappearance of the NCA carbonyl stretching band at 1780 and 1850 cm^{-1} confirmed complete NCA conversion. The degree of polymerisation (DP) was determined by ^{1}H NMR spectroscopy, based on the integration of four central methylene protons from 1,6-hexanediamine (δ = 1.24 and 1.38 ppm) and the methylene protons of PSar (δ = 4.57–3.73 ppm), yielding a DP of 30, closely matching the theoretical DP of 28 (Fig. S2). Size exclusion chromatography (SEC) analysis revealed a monomodal molecular weight distribution with a low dispersity ($Đ$ = 1.1), indicative of a well-controlled polymerisation process (Fig. S2). To introduce photoreactive functionality, PSar was chain-end modified with 2-isocyanatoethyl methacrylate *via* urea bond formation to introduce methacrylate groups (PSar-MA). The modification efficiency (>95%) was confirmed by ^{1}H NMR through the emergence of methacrylate vinyl proton signals at δ = 5.67 and 6.06 ppm (Fig. 1A). Additional confirmation was provided by diffusion-ordered spectroscopy (DOSY) NMR, which showed the same diffusion coefficients for the vinyl protons and PSar, consistent with successful incorporation of methacrylate groups into PSar (Fig. S2). FTIR spectra of PSar and PSar-MA further supported the modification, with the appearance of a characteristic peak at 1540 cm^{-1} attributed to C=C stretching vibrations (Fig. S1). SEC analysis of PSar-MA demonstrated that the polymer maintained its monomodal distribution and low dispersity ($Đ$ = 1.1) after functionalisation (Fig. S2).

4-Arm PEG-CA was synthesized from commercially available 4-arm poly(ethylene glycol) (4-arm PEG-OH; 2000 g mol^{-1}) which was end-functionalised with cinnamic acid (CA) *via* *N*,*N*′-dicyclohexylcarbodiimide (DCC)-mediated esterification to yield PEG-CA (Fig. 1B). Integration of the aromatic NMR proton signals of CA at δ = 7.38, 7.53 ppm relative to the PEG methylene protons at δ = 3.62 ppm (Fig. 1B and Fig. S3) confirmed successful end group modification exceeding 95%. DOSY NMR analysis further supported the conjugation, revealing a uniform shift in diffusion coefficients consistent with the formation of single-modified PEG species (Fig. S3). FTIR spectra of PEG and PEG-CA also confirmed successful functio-

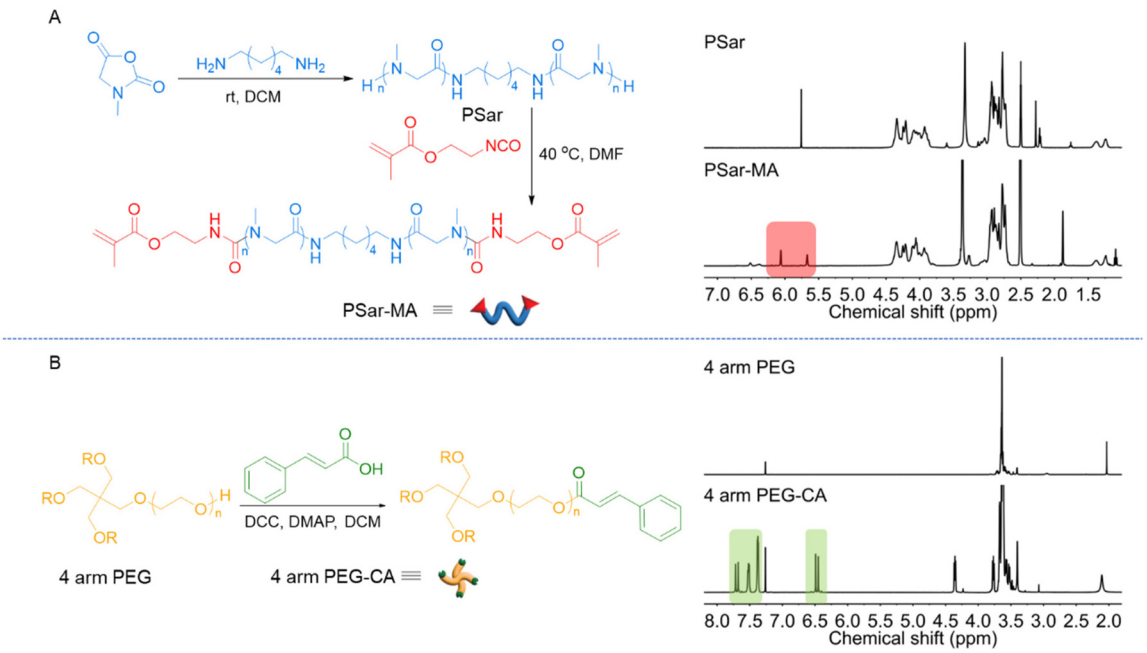

Fig. 1 Synthetic procedure for the synthesis of (A) PSar-MA and (B) 4 arm PEG-CA and their ^{1}H NMR spectra. Red and green boxes in the ^{1}H NMR spectra highlight reactive methacrylate (MA) and cinnamic acid (CA) end-groups. Full peak assignment available in Fig. S2 and S3.

This journal is © The Royal Society of Chemistry 2026

Open Access Article. Published on 03 december 2025. Downloaded on 16.5.2026. 03.44.44.
This article is licensed under a Creative Commons Attribution 3.0 Unported Licence.

nalisation, with characteristic signals (1700 cm^{-1}) corresponding to ester bond formation (Fig. S1). Size exclusion chromatography (SEC) analysis showed monomodal elution profiles with a low dispersity ($Đ$ = 1.1), indicating a homogeneous distribution of molecular weights (Fig. S3).

Rheological and swelling studies

Resins were formulated using PSar-MA and PEG-CA, with phenylbis(2,4,6-trimethylbenzoyl)-phosphine oxide (BAPO, 4 wt%) as the radical photoinitiator and *N*-methyl-2-pyrrolidone (NMP) as the solvent to facilitate solubility of the photo initiator. Initially curing experiments were carried out with the individual polymers to identify the required UV exposure time and inform the rheological investigation. While for PSar-MA gelation occurred within a few seconds, PEG-CA gelation was only observed after six hours (Fig. 2B and Fig. S4). The evolution of the viscoelastic properties of the hydrogels was then investigated through both time-dependent and frequency-dependent rheological measurements. Frequency sweep experiments were conducted at different curing times for a sample containing a one to one weight ratio of both polymers (SIN-1/1) to monitor the progressive formation of the dual-network structure (Fig. 2A). At 0 h, the storage modulus (G') and loss modulus (G'') were low and comparable at low frequencies, consistent with the typical behavior of liquid-like materials, indicating a weakly viscous liquid with limited chain interactions. After 0.5 h of curing, G' increased to 56 Pa, significantly higher than G'' across the frequency range, confirming the formation of the first network *via* radical crosslinking of PSar-MA. Upon extended curing (6 h), G' further increased to approximately 274 Pa and exhibited reduced frequency dependence, signifying the establishment of the secondary PEG-CA network. This evolution from a weakly viscous liquid to an viscoelastic gel highlights the sequential and independent network formation of PSar-MA and PEG-CA, a characteristic of the SIN design.

The composition-dependent photoresponse of the SIN hydrogels was further examined through time-sweep rheology under UV irradiation (Fig. S5). The UV light source (405 nm) was switched on after 60 s to establish an time zero baseline. Upon irradiation, both SIN-1/1 (PSar-MA 15 wt%, PEG-CA 15 wt%) and SIN-2/1 (PSar-MA 20 wt%, PEG-CA 10 wt%) exhibited a sharp rise in G', reaching the gel point almost simultaneously, indicating comparable photo-curing kinetics governed by the rapid polymerisation of PSar-MA. In contrast, SIN-1/2 (PSar-MA 10 wt%, PEG-CA 20 wt%) showed negligible change in G' throughout the measurement, confirming that an excess of PEG-CA significantly suppressed network formation within the observed irradiation period due to its low photoreactivity. These results demonstrate that the SIN hydrogel system features tunable, time-dependent network formation, in which PSar-MA governs the rapid initial gelation, while PEG-CA contributes gradually to long-term network reinforcement.

Next, single network hydrogel as well as SIN hydrogel samples were prepared using PSar-MA and PEG-CA formulations at the same polymer ratios (0/1, 1/0, 1/1, 1/2 and 2/1). Films were cast by pouring the resin into rectangular molds (H 0.8 mm × W 10 mm × L 20 mm) and irradiated with 405 nm UV light (2 mW cm^{-2}) for 16 hours. As suggested by the rheological measurements, it was hypothesised that rapid crosslinking of PSar-MA would establish the primary network, followed by slower PEG-CA crosslinking to form a secondary network (Fig. 3). After curing, the films were first dried in a vacuum oven until their weight remained constant, then swollen in DI water for 24 h to remove residual NMP and uncrosslinked components.

Swelling tests of the films in DI water were carried out to evaluate the water absorption capacity and degree of swelling. The gel fraction and swelling ratio of the PSar-MA and PEG-CA single networks as well as their corresponding SIN hydrogels exhibited distinct trends, influenced by differences in network composition, photoreactivity, and crosslinking mechanisms

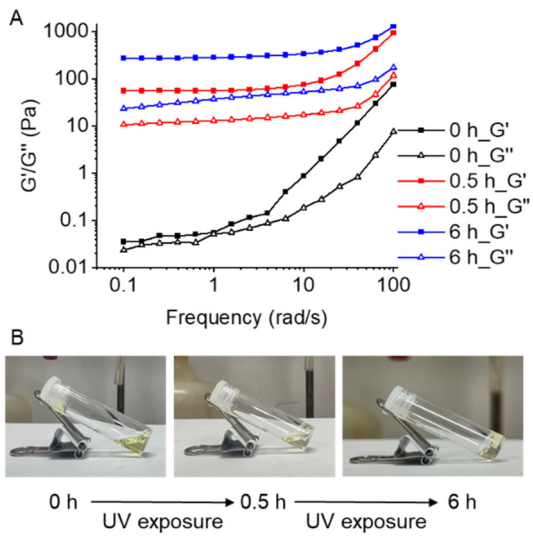

Fig. 2 (A) Frequency sweep showing the viscoelastic behavior of the SIN-1/1 hydrogel over a range of angular frequencies at constant strain, with curves measured at different UV (405 nm) exposure timepoints. Storage modulus (G', filled symbols) and loss modulus (G'', open symbols) (PSar-MA 15 wt%, PEG-CA 15 wt%, BAPO 4 wt%, NMP 70 wt%). (B) Gelation process of the PEG-CA hydrogel precursor solution over time (PEG-CA 15 wt%, BAPO 4 wt%, NMP 85 wt%).

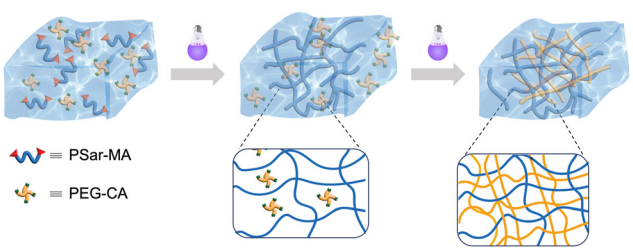

Fig. 3 Proposed SIN formation from PSar-MA and PEG-CA formulations.

Open Access Article. Published on 03 decembar 2025. Downloaded on 16.5.2026. 03.44.44.
This article is licensed under a Creative Commons Attribution 3.0 Unported Licence.

(Table S1). Triplicate measurements of the gel fraction showed similar values across all samples, approximately 74%, indicating comparable crosslinking efficiency. Samples cured for only 10 min displayed a gel fraction of 59 ± 4.9% in agreement with crosslinking of predominantly the PSar-MA network. In contrast, the swelling ratios varied more substantially with composition. A lower swelling ratio was observed with increasing PEG-CA content. For instance, the swelling ratio of PSar-SN was 5.4 ± 0.04, while that of PEG-SN was significantly lower at 1.8 ± 0.13. Among the SIN hydrogels, SIN-2/1 exhibited a swelling ratio of 3.7 ± 0.08, whereas the other SIN variants showed values in the range of 2.2–2.5. These lower swelling ratios at higher PEG-CA content suggest the formation of denser polymer networks. This is attributed to the tetrafunctional structure of PEG-CA and its 2 + 2 cycloaddition mechanism, which typically produces more uniform and tightly crosslinked networks compared to the free-radical polymerisation of the linear PSar-MA.[57–59]

To assess mechanical performance of the films, tensile testing was conducted to measure Young's modulus, elongation at break, and ultimate tensile strength of the hydrogels. For the tensile tests, the PSar-MA exhibited a Young's modulus of about 159 ± 44 kPa and a strain at break of 62 ± 15% kPa (Fig. 4A and Table 1). The PEG-CA single-network hydrogel showed a comparable modulus (115 ± 16 kPa) but significantly lower strain at break (16%). This is likely a consequence of the higher cross-link density of the PEG-CA network due to its 4-arm structure.[60] In contrast, the SIN-1/1 hydrogel demonstrated enhanced mechanical performance, with a strain at break of 98 ± 6% and a Young's modulus of 307 ± 54 kPa. This improvement in flexibility and toughness is attributed to the interpenetrating network architecture, which facilitates energy dissipation and more uniform stress distribution under load. When the ratio of the polymers was changed to 1/2 or 2/1 both tensile strength and elongation at break dropped suggesting optimal toughness and ductility for the SIN-1/1 (Fig. 4B and Table 1). These findings underline the importance of balanced network composition, with the 1/1 formulation providing the best synergy between the two polymer networks.

Compressive strength is critical for applications involving mechanical loading. As crosslinking density influences a hydrogel's resistance to deformation, compression tests were conducted to evaluate stiffness, stress at break, and energy dissipation across different network compositions. The compressive properties of PSar-MA, PEG-CA, and SIN hydrogels were assessed through stress–strain profiles and corresponding Young's moduli (Fig. 4C, D and Table 1). PSar-SN and PEG-SN exhibited moderate stiffness, with Young's moduli of 465 ± 20 kPa and 447 ± 66 kPa, respectively. However, their relatively low stress at break (184 ± 66 kPa for PSar-MA; 194 ± 49 kPa for PEG-CA) and limited strain at break (50%) suggest insufficient energy dissipation in single-network systems. In contrast, SIN hydrogels displayed markedly enhanced compressive properties. The interpenetrating architecture promoted effective load distribution and reduced localised failure, resulting in increased stiffness (Young's modulus up to >700 kPa) and stress at break exceeding 600 kPa. Further investigation into the role of network composition revealed a similar trend as for the tensile test with increased values for the SIN-1/1 (Fig. 4D and Table 1).

These results highlight the critical role of network composition in tuning the mechanical behaviour of the SIN hydrogels. The SIN-1/1 formulation consistently outperformed other ratios in both tensile and compressive tests, demonstrating a

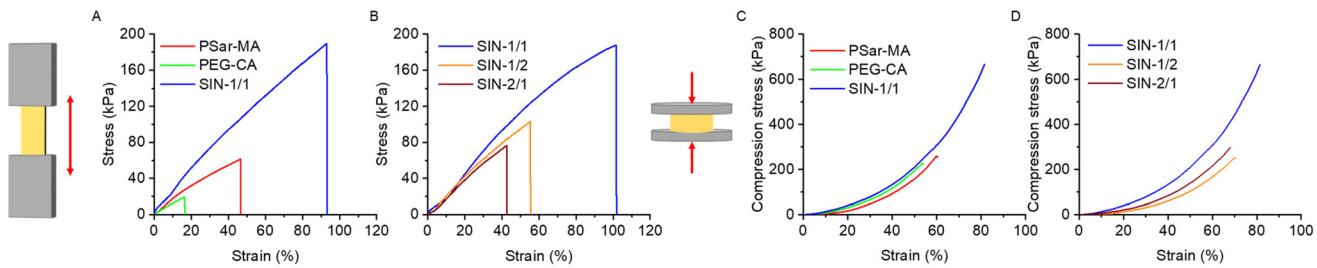

Fig. 4 (A) Stress–strain plot of PSar-MA, PEG-CA, and SIN; (B) stress–strain plot of SIN-1/1, SIN-1/2 and SIN-2/1; (C) compressive stress of PSar-MA, PEG-CA, SIN; (D) compressive stress of SIN-1/1, SIN-1/2, and SIN-2/1. Total polymers concentration 30 wt% in NMP, BAPO 4 wt%.

Table 1 Mechanical properties of single networks (SN) and simultaneous interpenetrating networks (SIN) (triplicate measurements)

Resin	Youngs modulus (tensile) (kPa)	Elongation at break (%)	Ultimate strength (kPa)	Youngs modulus (compression) (kPa)	Strain at break (%)	Ultimate compressive strength (kPa)
PSar-MA	159 ± 44	62 ± 15	63 ± 3	465 ± 20	51 ± 8	184 ± 66
PEG-CA	115 ± 16	16 ± 1	18 ± 1	447 ± 66	52 ± 5	194 ± 49
SIN-1/1	307 ± 54	98 ± 6	188 ± 3	728 ± 27	83 ± 1	648 ± 33
SIN-1/2	210 ± 22	53 ± 5	84 ± 17	403 ± 16	65 ± 8	212 ± 59
SIN-2/1	206 ± 15	43 ± 1	72 ± 4	735 ± 40	72 ± 5	340 ± 53

This journal is © The Royal Society of Chemistry 2026

Open Access Article. Published on 03 decembar 2025. Downloaded on 16.5.2026. 03.44.44.
This article is licensed under a Creative Commons Attribution 3.0 Unported Licence.

favourable balance of stiffness, strength, and extensibility. This study demonstrates the potential of compositionally optimised double-network PEG/PSar hydrogels for load-bearing biomedical applications, where precise mechanical performance is essential.

Cell compatibility

To evaluate the biological performance of the SIN hydrogels, we investigated their ability to support cell metabolic activity and proliferation of rat mesenchymal stem cells (rMSCs). rMSCs were seeded directly onto each hydrogel sample at 5×10^5 cells and incubated under standard culture conditions.[61] Seeding efficiency, metabolic activity, and IPNA content were measured to assess the cell compatibility of PSar-MA and PEG-CA single hydrogels as well as the SIN-1/1 hydrogel. All experiments were caried out in triplicate.

When comparing the cell seeding efficiency, a crucial indicator for successful tissue development, only 18.6 ± 1.3% of the initially seeded cells remained on the PSar-MA single network after 24 hours of incubation. The PEG-CA single network exhibited a 2-fold higher efficiency of 42.2 ± 1.0% at the same time point (Fig. 5A). Remarkably, the SIN-1/1 hydrogel demonstrated the highest seeding efficiency of 71.9 ± 1.3%, exceeding the PEG-CA by 1.7-fold and PSar-MA by 3.9-fold. Cell metabolic activity, as assessed on Day 1 (Fig. 5C), followed a similar trend: PEG-CA and SIN-1/1 hydrogels supported significantly higher cell viability compared to PSar-MA. Over time, the SIN-1/1 hydrogel maintained consistent metabolic activity from day 1 to day 10, similar to the PEG-CA hydrogel. Interestingly, PSar-MA, despite its low initial cell viability, exhibited a steady increase in metabolic activity throughout the culture period. By day 10, no significant differences in cell viability were observed among the three hydrogel types, suggesting that all are non-toxic and capable of supporting sustained cell growth.

To assess long-term proliferation, total DNA content was quantified after ten days using the Quanti-iT PicoGreen assay (Fig. 5B). SIN hydrogels exhibited significantly higher DNA content than both single-network hydrogels, indicating superior support for cell proliferation. While the reasons for this need to be studied in more depth, it is possible that the balanced combination of network elasticity and hydrophilicity of the SIN-1/1 network creates a more favourable microenvironment for rMSC adhesion and proliferation, leading to higher DNA content.[62,63] These results highlight the SIN hydrogel's enhanced ability to promote cell adhesion, viability, and expansion, supporting its potential in tissue engineering and regenerative medicine.

We further investigated the impact of SIN hydrogel composition on cell behaviour by comparing formulations with varying PSar-MA/PEG-CA ratios (1/1, 1/2, and 2/1). Seeding efficiency remained consistent across all variants (Fig. S6). All SIN compositions supported a gradual increase in cell metabolic activity over time, with no significant differences observed by Day 10 (Fig. S7). DNA quantification results mirrored this trend, with similar values across all formulations (Fig. S8).

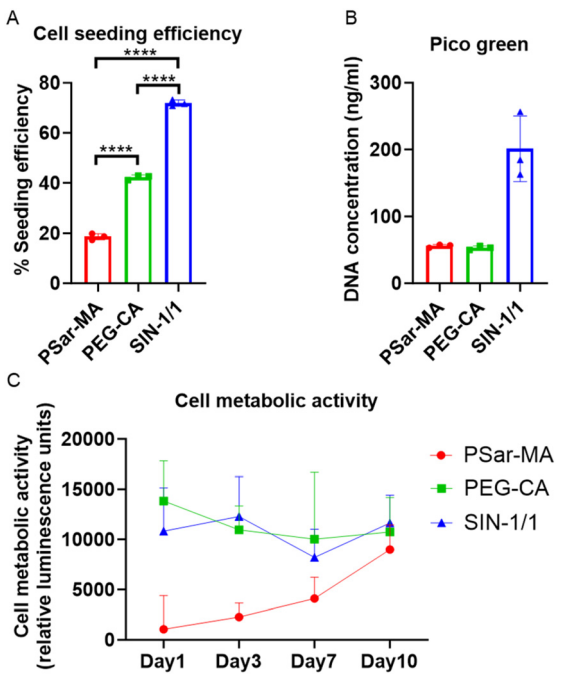

Fig. 5 (A) Percentage of cell seeding efficacy at 24 h (rMSC). * represent statistical differences (at $p < 0.05$) between the various groups indicating that the SIN hydrogel has a highest seeding efficiency. (B) DNA concentration per hydrogel was determined after 10 days in cell culture. (C) Cellular metabolic activity per hydrogel determined at day 1, 3, 7, and 10 in cell culture. Data shown represent three individual MSC biological repeats ($n = 3$ per biological repeat).

Conclusions

PSar and PEG precursors were successfully synthesised and efficiently functionalised with methacrylate and cinnamic acid groups, respectively. Both were photo-crosslinked individually and simultaneously. Due to the markedly different crosslinking kinetics of the PSar-MA and PEG-CA, polymer blends afforded Simultaneously Interpenetrating Networks (SIN). Overall, it was found that the SIN hydrogels outperformed the single-network systems for all tested mechanical properties. Moreover, SINs promoted higher initial cell adhesion, sustained metabolic activity, and enhanced proliferation of rMSCs. These findings indicate that the synergistic combination of PSar-MA and PEG-CA within the SIN network provides a more favourable microenvironment for cell growth, suggesting their strong potential for applications in tissue engineering and regenerative medicine.

Conflicts of interest

There are no conflicts to declare.

Open Access Article. Published on 03 decembar 2025. Downloaded on 16.5.2026. 03.44.44.
This article is licensed under a Creative Commons Attribution 3.0 Unported Licence.

Data availability

The data supporting this article have been included as part of the supplementary information (SI). Supplementary information: polymer ^{1}H NMR, FTIR, DOSY NMR spectra and SEC traces; table resin composition and swelling properties; cell data for SIN networks. See DOI: https://doi.org/10.1039/d5py01018g.

Acknowledgements

This work was financially supported by RCSI/Soochow StAR International programme 2023.

References

1 E. M. Ahmed, *J. Adv. Res.*, 2015, **6**, 105.
2 P. Sánchez-Cid, M. Jiménez-Rosado, A. Romero and V. Pérez-Puyana, *Polymers*, 2022, **14**, 3023.
3 S. Correa, A. K. Grosskopf, H. Lopez Hernandez, D. Chan, A. C. Yu, L. M. Stapleton and E. A. Appel, *Chem. Rev.*, 2021, **121**, 11385.
4 S. Bashir, M. Hina, J. Iqbal, A. H. Rajpar, M. A. Mujtaba, N. A. Alghamdi, S. Wageh, K. Ramesh and S. Ramesh, *Polymers*, 2020, **12**, 2702.
5 J. Li and D. J. Mooney, *Nat. Rev. Mater.*, 2016, 16071.
6 S. Kim, S. Min, Y. S. Choi, S.-H. Jo, J. H. Jung, K. Han, J. Kim, S. An, Y. W. Ji, Y.-G. Kim and S.-W. Cho, *Nat. Commun.*, 2022, **13**, 1692.
7 Y. Zhang, Y. Xu and J. Gao, *Biomater. Sci.*, 2023, **11**, 3784.
8 S. Martin-Saldaña, M. Al Waeel, A. M. Alsharabasy, A. Daly and A. Pandit, *Matter*, 2022, **5**, 3659.
9 A. D. Augst, H. J. Kong and D. J. Mooney, *Macromol. Biosci.*, 2006, **6**, 623.
10 D. Ji, J. M. Park, M. S. Oh, T. L. Nguyen, H. Shin, J. S. Kim, D. Kim, H. S. Park and J. Kim, *Nat. Commun.*, 2022, **13**, 3019.
11 Z. Luo, Y. Wang, J. Li, J. Wang, Y. Yu and Y. Zhao, *Adv. Funct. Mater.*, 2023, **33**, 2306554.
12 Y. Ren, Q. Wang, W. Xu, M. Yang, W. Guo, S. He and W. Liu, *Int. J. Biol. Macromol.*, 2024, **279**, 135019.
13 S. Wang, S. Tavakoli, R. P. Parvathaneni, G. N. Nawale, O. P. Oommen, J. Hilborn and O. P. Varghese, *Biomater. Sci.*, 2022, **10**, 6399.
14 B. Salahuddin, S. Wang, D. Sangian, S. Aziz and Q. Gu, *ACS Appl. Bio Mater.*, 2021, **4**, 2886.
15 H. A. Nawaz, K. Schröck, M. Schmid, J. Krieghoff, I. Maqsood, C. Kascholke, C. Kohn-Polster, M. Schulz-Siegmund and M. C. Hacker, *J. Mater. Chem. B*, 2021, **9**, 2295.
16 Z. Yi, L. Qi, Yu Han, S. Lei, C. Xiang, P. Qian, Z. Yabin and H. Ruixia, *Front. Chem.*, 2024, **12**, 1376799.
17 M. M. R. Khan and M. M. H. Rumon, *Gels*, 2025, **11**, 88.
18 Y. Wang, R. Zhang, Z. Qiao, B. Dou, H. Xu, F. Meng and J. Huang, *ACS Appl. Bio Mater.*, 2025, **8**, 2356.
19 F. Milos and A. del Campo, *Adv. Mater. Interfaces*, 2024, **11**, 2400404.
20 Z. Wang, Q. Ye, S. Yu and B. Akhavan, *Adv. Healthcare Mater.*, 2023, **12**, 2300105.
21 J. Shi, L. Yu and J. Ding, *Acta Biomater.*, 2021, **128**, 42.
22 S. Liu, T. Jiang, R. Guo, C. Li, C. Lu, G. Yang, J. Nie, F. Wang, X. Yang and Z. Chen, *ACS Appl. Bio Mater.*, 2021, **4**, 2769–2780.
23 Y. Gao, M. Joshi, Z. Zhao and S. Mitragotri, *Bioeng. Transl. Med.*, 2024, **9**, e10600.
24 Z. Wang, Q. Ye, S. Yu and B. Akhavan, *Adv. Healthcare Mater.*, 2023, **12**, 2300105.
25 M. A. Daniele, A. A. Adams, J. Naciri, S. H. North and F. S. Ligler, *Biomaterials*, 2014, **35**, 1845.
26 D. A. Rennerfeldt, A. N. Renth, Z. Talata, S. H. Gehrke and M. S. Detamore, *Biomaterials*, 2013, **34**, 8241.
27 A. S. Abu Lila, H. Kiwada and T. Ishida, *J. Controlled Release*, 2013, **172**, 38.
28 Y. Ju, W. S. Lee, E. H. Pilkington, H. G. Kelly, S. Li, K. J. Selva, K. M. Wragg, K. Subbarao, T. H. O. Nguyen, L. C. Rowntree, L. F. Allen, K. Bond, D. A. Williamson, N. P. Truong, M. Plebanski, K. Kedzierska, S. Mahanty, A. W. Chung, F. Caruso, A. K. Wheatley, J. A. Juno and S. J. Kent, *ACS Nano*, 2022, **16**, 11769.
29 B.-M. Chen, T.-L. Cheng and S. R. Roffler, *ACS Nano*, 2021, **15**, 14022.
30 A. Birke, J. Ling and M. Barz, *Prog. Polym. Sci.*, 2018, **81**, 163.
31 H. Bayraktutan, R. J. Kopiasz, A. Elsherbeny, M. Martinez Espuga, N. Gumus, U. C. Oz, K. Polra, P. F. McKay, R. J. Shattock, P. Ordóñez-Morán, A. Mata, C. Alexander and P. Gurnani, *Polym. Chem.*, 2024, **15**, 1862.
32 X. Yao, C. Sun, F. Xiong, W. Zhang, W. Yao, Y. Xu, W. Fan and F. Huo, *ACS Appl. Mater. Interfaces*, 2024, **16**, 19472.
33 D. Skoulas, S. Fattah, D. Wang, S. A. Cryan and A. Heise, *Macromol. Biosci.*, 2022, **22**, e2200175.
34 S. Wang, M.-Y. Lu, S.-K. Wan, C.-Y. Lyu, Z.-Y. Tian, K. Liu and H. Lu, *J. Am. Chem. Soc.*, 2024, **146**, 5678.
35 B. Weber, A. Birke, K. Fischer, M. Schmidt and M. Barz, *Macromolecules*, 2018, **51**, 2653.
36 M. Yang, Z.-C. Zhang, F.-Z. Yuan, R.-H. Deng, X. Yan, F.-B. Mao, Y.-R. Chen, H. Lu and J.-K. Yu, *Bioact. Mater.*, 2023, **19**, 678.
37 N. Parvin, V. Kumar, S. W. Joo and T. K. Mandal, *Materials*, 2024, **17**, 3813.
38 A. Revete, A. Aparicio, B. A. Cisterna, J. Revete, L. Luis, E. Ibarra, E. A. Segura González, J. Molino and D. Reginensi, *Int. J. Biomater.*, 2022, 3606765.
39 J. Ye, S. Fu, S. Zhou, M. Li, K. Li, W. Sun and Y. Zhai, *Eur. Polym. J.*, 2020, **139**, 110024.
40 F. L. C. Morgan, I. A. O. Beeren, J. Bauer, L. Moroni and M. B. Baker, *J. Am. Chem. Soc.*, 2024, **146**, 27499.
41 M. Cosgrave, K. Kaur, C. Simpson, Ł. Mielańczyk, C. Murphy, R. D. Murphy and A. Heise, *Biomacromolecules*, 2025, **26**, 670.

This journal is © The Royal Society of Chemistry 2026

Open Access Article. Published on 03 decembar 2025. Downloaded on 16.5.2026. 03.44.44.
This article is licensed under a Creative Commons Attribution 3.0 Unported Licence.

42 E. Walejewska, F. P. W. Melchels, A. Paradiso, A. McCormack, K. Szlazak, A. Olszewska, M. Srebrzynski and W. Swieszkowski, *Biomacromolecules*, 2024, **25**, 188.
43 J. P. Gong, *Soft Matter*, 2010, **6**, 2583.
44 A. P. Dhand, M. D. Davidson, J. H. Galarraga, T. H. Qazi, R. C. Locke, R. L. Mauck and J. A. Burdick, *Adv. Mater.*, 2022, **34**, 2202261.
45 P. Seth, J. Friedrichs, Y. D. P. Limasale, N. Fertala, U. Freudenberg, Y. Zhang, A. Lampel and C. Werner, *Adv. Healthcare Mater.*, 2025, **14**, 2402656.
46 S. Ishikawa, K. Iijima, D. Matsukuma, Y. Asawa, K. Hoshi, S. Osawa and H. Otsuka, *Chem. Mater.*, 2020, **32**, 2353.
47 K. K. V. G. Sinad, R. C. Ebubechukwu and C. K. Chu, *J. Mater. Chem. B*, 2023, **11**, 11460.
48 Z. Zou, B. Zhang, X. Nie, Y. Cheng, Z. Hu, M. Liao and S. Li, *RSC Adv.*, 2020, **10**, 39722.
49 S. O'Brien, R. P. Brannigan, R. Ibanez, B. Wu, J. O'Dwyer, F. J. O'Brien, S. Cryan and A. Heise, *J. Mater. Chem. B*, 2020, **8**, 7785.
50 A. P. Dhand, M. D. Davidson, J. H. Galarraga, T. H. Qazi, R. C. Locke, R. L. Mauck and J. A. Burdick, *Adv. Mater.*, 2022, **34**, 2202261.
51 P. Demianenko, B. Minisini, M. Lamrani and F. Poncin-Epaillard, *Mater. Today Commun.*, 2015, **4**, 1.
52 M. S. Silverstein, *Polymer*, 2020, **207**, 122929.
53 L. Zhao, R. Yu, Y. He, M. Zhang, F. Tian, L. Wang, Y. Zhao and W. Huang, *Addit. Manuf.*, 2024, **79**, 103904.
54 Z. O. Shah, A. Trengove, A. J. O'Connor, J. F. Quinn and K. Kempe, *Macromol. Mater. Eng.*, 2023, **309**, 2300210.
55 S. An, C. Intini, D. O'Shea, J. E. Dixon, Y. Zheng and F. J. O'Brien, *Mater. Today Bio*, 2025, **30**, 101382.
56 R. N. Power, B. L. Cavanagh, J. E. Dixon, C. M. Curtin and F. J. O'Brien, *Int. J. Mol. Sci.*, 2022, **23**, 1460.
57 T. Matsunaga, T. Sakai, Y. Akagi, U. Chung and M. Shibayama, *Macromolecules*, 2009, **42**, 1344–1351.
58 L. Zhao, *J. Mater. Chem. C*, 2023, **11**, 2826.
59 M. Okihara, K. Okuma, A. Kawamura and T. Miyata, *Gels*, 2022, **8**, 183.
60 Y. Huang, P. B. Jayathilaka, M. S. Islam, C. B. Tanaka, M. N. Silberstein, K. A. Kilian and J. J. Kruzic, *Acta Biomater.*, 2022, **138**, 301.
61 B. Podhorská, E. Chylíková-Krumbholcová, J. Dvořáková, M. Šlouf, L. Kobera, O. Pop-Georgievski, M. Frejková, V. Proks, O. Janoušková, M. Filipová and P. Chytil, *Macromol. Biosci.*, 2024, **24**, 2300266.
62 O. Chaudhuri, J. Cooper-White, P. A. Janmey, D. J. Mooney and V. B. Shenoy, *Nature*, 2020, **584**, 535.
63 X. Tong and F. Yang, *Biomaterials*, 2014, **35**, 1807.